

Domain Growth in Chiral Phase Transitions: Inertial Dynamics

Awaneesh Singh¹, Sanjay Puri¹ and Hiranmaya Mishra^{1,2}

¹School of Physical Sciences, Jawaharlal Nehru University, New
Delhi-110067, India.

²Theory Division, Physical Research Laboratory, Navrangpura,
Ahmedabad-380009, India.

Abstract

We investigate the kinetics of phase transition for chiral symmetry breaking after a collision with high-energy heavy ions. We use a Langevin description for domain growth kinetics in the chiral phase transition. The Langevin equation of motion for the order parameter field includes dissipation and the *inertial term* with a Gaussian random force. We study the far-from-equilibrium ordering dynamics subsequent to a quench from the massless quark phase to the massive quark phase and discuss the effect of dissipation on the dynamic magnification. After a discussion on the growth of the bubble, we introduce the assumption of scale and to show how a dynamic correlation length emerges. We find a simple length scale corresponding to the Allen-Chan (AC) growth law i.e., $L(t) \sim t^{1/2}$.

1 Introduction

Strongly interacting hadronic matter is expected to undergo a phase transition at sufficiently high temperature and/or baryon density. For vanishing baryon density, this is a prediction from *abinitio* calculations like the lattice simulation of the *quantum chromo dynamics* (QCD) while for finite baryon density, this is expected from different effective models of the strongly interacting system. Heavy ion collisions provide an opportunity to scrutinize the phase structure of QCD experimentally. The high temperature and low baryon density phase was explored in the *relativistic heavy ion collision* (RHIC) experiments at Brookhaven and it will be further studied in the *large hadron colliders* (LHC) experiments. The planned experiments like *beam energy scan* (BES) at RHIC [1], *compressed baryonic matter* (CBM) at GSI [2] and *nuclotron-based ion collider facility* (NICA) at Dubna [3] intend to study different aspects of the thermodynamic properties of QCD at finite chemical potential, such as the expected critical point of QCD, first order phase transition as well as the mixed phase structure.

However, it is challenging to extract the thermodynamic properties of quark hadron phase transition from the nuclear collision experiments. Apart from the system size being small, the dynamics here is rather fast and can prevent the thermal equilibrium being established globally. Therefore, it is likely that the nonequilibrium effects play an important role in the evolution of the fireball. It may be emphasized here that an understanding of the equilibrium phase diagram is not sufficient to surmise the properties of such a system. One also has to understand the kinetic process that drive the phase

transition and the properties of the nonequilibrium structures that the system goes through on its way to reach equilibrium [4]. In this regard, both the *critical dynamics* and the *far-from-equilibrium kinetics* of chiral transition has attracted recent attention. In the study of critical dynamics (i.e., the time-dependent behavior in the vicinity of the critical point), much interest has been on the signatures of the *critical end point* (CEP) of QCD [5, 6, 7, 8]. In this paper, we focus on the second aspect: the far-from-equilibrium kinetics i.e., the evolution of the system after a quench from a disordered phase at high temperature to an ordered phase of low temperature with nonvanishing quark antiquark condensates.

In this context, the relaxation to equilibrium using Langevin equation has been attempted in Ref. [9], where the authors studied the early time dynamics of the *spinodal decomposition* and the effect of dissipation on the spinodal instability. Further, the bubble nucleation kinetics in chiral transition was studied in Ref. [10]. A *time-dependent Ginzburg Landau* equation (TDGL) was derived in Ref. [11] starting from a non-ideal, nonrelativistic hydrodynamics for coupled order parameters. The authors here clarified the effect of viscosity in the ordering kinetics. Further, in Ref. [12], the amplification of the spinodal fluctuation was studied within a fluid dynamical model for the nuclear collisions. Here, the study was mostly focused on the evolution in the linearized regime which showed an exponential growth of the initial fluctuations.

We have recently attempted the far-from-equilibrium kinetics of chiral phase transition using a TDGL equation [13], which was complementary

to the studies of Refs. [9, 10, 11, 12] and investigated the late stages of phase separation kinetics in quark matter. The Ginzburg Landau free energy functional was obtained from an expansion of the thermodynamic potential of a two flavor *Nambu-Jona-Lasinio* (NJL) model. The nonlinearities in the evolution equation made the exponential growth of the initial fluctuations stabilize. The quenching scenario was studied where the quenching is done through the second order as well as the first order line in the phase diagram. The domain growth in both types of quenching was studied and different quantitative features of the coarsening morphologies were also discussed.

Let us note that the phenomenological TDGL equation which models the overdamped (relaxational) dynamics of order parameter field to the minimum of the thermodynamic potential [14] is first-order in time derivative. However, a microscopic derivation of the equation in a relativistic field theory using e.g., *closed time path Green's function* (CTPGF) leads to a second-order stochastic equation. Such a derivation has been done for scalar field theory [15, 16, 17]. A second order TDGL equation has also been derived for NJL model in Ref. [18] using CTPGF method. More recently, Langevin equation has been derived for the chiral order parameter field in a sigma model including quark degrees of freedom in Ref. [19]. Here, the authors use influence functional method and calculate the explicit form of the damping coefficient as well as the form of noise correlators that appear in the Langevin equation which again is a second-order equation in time. This has been further used to discuss relaxational dynamics of the order parameter near the critical point [20, 21]. In condensed matter literature such a second order

temporal derivative term is also known as the *inertial term*. In this context, it is relevant to investigate the effect of the inertial term in the dynamical equation on the the late stage of ordering kinetics for the chiral transition. We intend to look into and investigate in which physical condition which evolution equation need to be considered.

This paper is organized as follows. In Sec. 2, for the sake of completeness, we recapitulate the NJL model effective potential and the corresponding mapping to the M^6 Landau potential discussed in Ref. [13]. This is used to write down the Langevin equation for the order parameter evolution with the inertial term in Sec. 3. In Sec. 4, we study the kinetics of chiral phase transition with a variety of different quenches and focus on the late stage pattern formation dynamics. We discuss the effect of dissipation coefficient on the dynamics. Finally, this paper concludes with a summary and discussion in Sec. 5.

2 Thermodynamic potential and phase diagram

To discuss the kinetics of chiral phase transition, we model chiral symmetry breaking in strong interaction in the 2-flavor NJL model. The thermodynamic potential in terms of constituent mass is given as [13]

$$\begin{aligned} \tilde{\Omega}(M, \beta, \mu) = & -\frac{12}{(2\pi)^3\beta} \int d\vec{k} \left\{ \ln \left[1 + e^{-\beta(\sqrt{k^2+M^2}-\mu)} \right] \right. \\ & \left. + \ln \left[1 + e^{-\beta(\sqrt{k^2+M^2}+\mu)} \right] \right\} \\ & - \frac{12}{(2\pi)^3} \int d\vec{k} \left(\sqrt{k^2+M^2} - k \right) + \frac{M^2}{4G}. \end{aligned} \quad (1)$$

Here, we have taken vanishing current quark mass $m = 0$, and introduce $M = -2g\rho_s$, with $\rho_s = \langle \bar{\psi}\psi \rangle$ being the scalar density and $g = G[1 + 1/(4N_c)]$. We have taken the four-fermion coupling $G = 5.0163 \times 10^{-6} \text{ MeV}^{-2}$ [22].

Close to the phase boundary, the potential in Eq. (1) may be expanded as a Ginzburg-Landau (GL) potential in the order parameter M :

$$\tilde{\Omega}(M) = \tilde{\Omega}(0) + \frac{a}{2}M^2 + \frac{b}{4}M^4 + \frac{d}{6}M^6 + O(M^8) \equiv f(M), \quad (2)$$

correct upto logarithmic factors [23]. In the following, we consider the expansion of $\tilde{\Omega}(M)$ upto the M^6 -term. This will prove adequate to recover the phase diagram in the NJL model [13]. The first two coefficients in Eq. (2) can be obtained by comparison with Eq. (1) as

$$\begin{aligned} \tilde{\Omega}(0) &= -\frac{6}{\pi^2\beta} \int_0^\Lambda dk \, k^2 \{ \ln [1 + e^{-\beta(k-\mu)}] + \ln [1 + e^{-\beta(k+\mu)}] \}, \\ a &= \frac{1}{2G} - \frac{3\Lambda^2}{\pi^2} + \frac{6}{\pi^2} \int_0^\Lambda dk \, k \left[\frac{1}{1 + e^{\beta(k-\mu)}} + \frac{1}{1 + e^{\beta(k+\mu)}} \right]. \end{aligned} \quad (3)$$

We treat the higher coefficients as phenomenological parameters, which are obtained by fitting $\tilde{\Omega}(M)$ in Eq. (2) to the integral expression for $\tilde{\Omega}$ in Eq. (1). There are two free parameters in the microscopic theory (μ and T), so we consider the M^6 -GL potential with parameters b and d . For stability, we require $d > 0$. The phase diagram resulting from Eq. (2) is shown in Fig. 1.

The gap equation, $f'(M) = aM + bM^3 + dM^5 = 0$ yields the three solutions for the order parameter as ($M_0 = 0$ and $M_\pm^2 = (-b \pm \sqrt{b^2 - 4ad})/2d$). In Fig. 1 we show the phase diagram for the GL potential in $[b/(d\Lambda^2), a/(d\Lambda^4)]$ -space. For $b > 0$, the transition is second-order. The stationary points are $M = 0$ (for $a > 0$) or $M = 0, \pm M_+$ (for $a < 0$). For $a < 0$, the preferred

equilibrium state is the one with massive quarks [24]. Next, for $b < 0$, the corresponding solutions of the gap equations are (i) $M = 0$, for $a > b^2/(4d)$, (ii) $M = 0, \pm M_+, \pm M_-$, for $b^2/(4d) > a > 0$, and (iii) $M = 0, \pm M_+$, for $a < 0$. As we reduce a from higher values, 5 solutions appear at $a = b^2/4d$. However, this does not correspond to a phase transition. On further reduction of a , we obtain a first-order phase transition occurs at $a_c = 3b^2/(16d)$. The order parameter jumps discontinuously from $M = 0$ to $M = \pm M_+$, where $M_+ = [3|b|/(4d)]^{1/2}$. The tricritical point is located at $b_{\text{tcp}} = 0, a_{\text{tcp}} = 0$. In Fig. 1, the open symbols denote 4 combinations of $(b/(d\Lambda^2), a/(d\Lambda^4))$, chosen to represent qualitatively different shapes of the GL potential. The equation for the first order transition line (I) is $a_c = 3|b|^2/(16d)$, and for the second order transition line (II) is $a_c = 0$. The dashed lines denote the spinodals S_1 and S_2 , with equations $a_{S_1} = 0$ and $a_{S_2} = |b|^2/(4d)$. The typical forms of the Landau potential in various regions are shown in the Fig. 1. The cross denotes the point where we quench the system for $b < 0$.

3 The Dynamical Equation

We intend to investigate the time-dependent evolution of the order parameter $M(r, t)$ and its approach to equilibrium within the framework of the Langevin dynamics. The evolution of the system is described by the equation:

$$\frac{\partial^2}{\partial t^2} M + \gamma \frac{\partial}{\partial t} M + \frac{\delta \Omega[M]}{\delta M} = \theta(\vec{r}, t). \quad (4)$$

It is based on the construction of a coarse-grained free energy functional $\Omega[M]$ for the configuration of the order parameter field $M(\vec{r}, t)$ from a given

effective potential $f(M)$ as

$$\Omega[M] = \int d\vec{r} \left[\frac{a}{2} M^2 + \frac{b}{4} M^4 + \frac{d}{6} M^6 + \frac{K}{2} (\vec{\nabla} M)^2 \right]. \quad (5)$$

Here K measures the energy cost of spatial inhomogeneities at the domain interface. We substitute Eq. (5) in Eq. (4) and introduce dimensionless variables

$$\begin{aligned} M &= M_0 M', & M_0 &= \sqrt{|a|/|b|}, \\ \vec{r} &= \xi \vec{r}', & \xi &= \sqrt{K/|a|}, \\ t &= t_0 t', & t_0 &= 1/\sqrt{|a|}, \\ \theta &= |a| M_0 \theta', & \gamma' &= \gamma t_0. \end{aligned} \quad (6)$$

Dropping primes, we then have the dimensionless form of the evolution equation:

$$\frac{\partial^2}{\partial t^2} M + \gamma \frac{\partial}{\partial t} M = -\text{sgn}(a)M - \text{sgn}(b)M^3 - \lambda M^5 + \nabla^2 M + \theta(\vec{r}, t), \quad (7)$$

where $\text{sgn}(x) = x/|x|$ and $\lambda = |a|d/|b|^2 > 0$. The dissipation coefficient, γ (in units of t_0) can be considered as a response coefficient that defines a time scale for the system. The term $\nabla^2 M$ arises due to spatial inhomogeneity in the system. The function $\theta(\vec{r}, t)$ represents a stochastic force which is assumed to be a Gaussian and white noise, so that $\langle \theta(\vec{r}, t) \rangle = 0$ and $\langle \theta(\vec{r}', t') \theta(\vec{r}'', t'') \rangle = 2\epsilon \delta(\vec{r}' - \vec{r}'') \delta(t' - t'')$ [25], where ϵ is the noise strength. In general, the actual form of γ and θ could be more complicated [26]. However, for simplicity, in this exploratory study we chose the simple form of Eq. (7) which allows a clear distinction and comparison of the roles played by γ and the inertial term in the evolution dynamics.

Here we will consider a system (disordered phase) which becomes thermodynamically unstable when it is rapidly quenched below the critical temperature (T_c). Subsequent evolution of the system is characterized by the emergence and growth of domains (ordered phase). In the context of Fig. 1, it corresponds to (say) a quench from $a > a_c$ to $a < a_c$ at a fixed value of b . The unstable homogeneous state (with $M \simeq 0$) evolves via the emergence and growth of domains rich in the preferred phase (with $M = \pm M_+$).

In this paper, we have presented our results in dimensionless units of space and time. One can obtain the corresponding physical units by multiplying with the appropriate dimensional length-scale ξ and time-scale t_0 . For this, we need to estimate the strength of the interfacial energy K . We calculate the surface tension: $\sigma = \sqrt{K}(|a|^{3/2}/|b|) \int dz (dM/dz)^2$. For quark matter, σ is poorly known and varies from 10-100 MeV/fm² at small temperatures [27] – we take $\sigma \simeq 50$ MeV/fm². For example at $T = 10$ MeV and $\mu = 321.75$ MeV, we estimate $\xi = \sqrt{K/|a|} \simeq 2.8$ fm and $t_0 = 1/\sqrt{|a|} \simeq 5.1$ fm [13, 28].

In the following, we discuss the numerical results related to the ordering dynamics in the context of the phase diagram in Fig. 1 for two different situations. First, we study the phase-transition kinetics by quenching through the second-order line (II). The corresponding parameter values are $(a/\Lambda^2, b, d\Lambda^2) = (-1.6 \times 10^{-2}, 9 \times 10^{-2}, 7.1 \times 10^{-2})$ with $\lambda = |a|d/|b|^2 = 0.14$. This set of GL parameters correspond to $(\mu, T) = (231.6, 85)$ MeV [13]. Here the system evolves via spinodal decomposition. Next, we do the quenching so as to probe the metastable region of the phase diagram. This is achieved by shallow quenching through the first-order line (I) in Fig. 1, i.e., quenching to

the region between I and S_1 (marked by an arrow). Here, the system evolves via *nucleation and growth* of the droplets of favored phases. This case is studied using the parameter values $(a/\Lambda^2, b, d\Lambda^2) = (3.539 \times 10^{-3}, -0.101, 0.402)$ with $\lambda = 0.14$. It corresponds to the parameter pair $(\mu, T) = (322.8, 10)$ MeV [13]. This point is marked by a cross in the phase diagram of Fig. 1.

4 Kinetics of Chiral Transitions

4.1 Case with $b > 0$

In this case, we consider deep quenches through the second-order line (II). The chiral transition occurs when we quench from $a > 0$ (with $M = 0$) to $a < 0$, where the free energy has a double-well structure (cf. Fig. 1). The chirally-symmetric phase is now unstable, and evolves to the stable massive phase via the spinodal decomposition. The appropriate form of the evolution equation is

$$\frac{\partial^2}{\partial t^2} M + \gamma \frac{\partial}{\partial t} M = M - M^3 - \lambda M^5 + \nabla^2 M + \theta(\vec{r}, t). \quad (8)$$

We solve Eq. (8) numerically using a simple Euler-discretization scheme with initial velocity $\partial M / \partial t = 0$. The initial state of the system i.e., $M(r, 0)$ is prepared in a homogeneous state by assigning, to each lattice site, a random number uniformly distributed in the interval $[-0.25, +0.25]$. This is implemented on a 3- d lattice of size N^3 ($N = 256$), with periodic boundary conditions in all directions. For all results in this paper, we used the mesh sizes $\Delta x = 1.0$ and $\Delta t = 0.1$ obtained from the linear stability analysis of Eq. (8). The thermal noise $\theta(\vec{r}, t)$ is mimicked by uniformly-distributed

random numbers between $[-A_n, A_n]$; where $A_n = 0.5$ corresponding to $\epsilon = A_n^2(\Delta x)^d \Delta t/3 = 0.008$ [13].

In Fig. 2 we show the evolution of an initially disordered state to Eq. (8). To study the effect of dissipation, we choose $\gamma = 0, 0.4$, and 1.0 . After the quench, system rapidly evolves into domains of massive phase with $M \simeq -M_+$ and $M \simeq M_+$ via spinodal decomposition. The snapshots show the evolution of a preferred massive quark phase ($M = M_+$) at $t = 10, 50$ and 100 . The frames are the cross-section of the 3- d snapshots at $z = N/2$. As expected, the dissipation coefficient γ controls the rapid growth achieved due to the inertial term in Eq. (8). For $\gamma = 0$, the inertial term is prevailing and therefore, we observed a rapid growth of domains of the massive phases. These domains are destroyed due to the oscillatory behavior of the system in few time steps shortly.

However, the increasing value of γ reduces the effect of inertial term and makes the system dissipative i.e., the system will now relaxed to equilibrium. For large dissipation (e.g. $\gamma = 1$), the growth process is analogous to coarsening dynamics observed in Ref. [13]. Coarsening is driven by kinks, so we can use the dynamics of kinks to obtain a good understanding of this evolution. The domain scale obeys the Allen-Cahn (AC) growth law, $L(t) \sim t^{1/2}$. In general, the interface velocity $v \sim dL/dt \sim 1/L$, where L^{-1} measures the local curvature of the interface.

The system is characterized by a single length scale $L(t)$ as the pattern morphology does not change in time apart from a scale factor. The morphology is quantitatively studied using the *correlation function*, $C(\vec{r}, t)$. The

existence of the characteristic scale results in a *dynamical scaling* of the correlation function: $C(\vec{r}, t) = g(r/L)$. While microscopic techniques can be used to measure $C(\vec{r}, t)$, scattering experiments probe its Fourier transform, called the *structure factor*, $S(\vec{k}, t)$. The structure factor is also related to a time-independent form or a dynamical scaling form: $S(\vec{k}, t) = L^d f(kL)$, where $g(x)$ and $f(p)$ are the scaling functions [4, 13, 25].

In Fig. 3, we plot $L(t)$ vs. t on a log-log scale. The length scale $L(t)$ is obtained as the distance over which the correlation function decays to half its maximum value (at $r = 0$). The large γ value reduces the effect of inertia on the system and therefore, the quenching scenario in this regime is similar to the one with M^4 potential (cf. Ref. [13] for the overdamped limit). In this case the domain growth data is consistent with the AC growth law, $L(t) \sim t^{1/2}$ at late stages. However, at smaller $\gamma = 0, 0.2$, we observed an explosive domain growth with higher growth exponent. The dependence of the spinodal time-scale (t_{sp}) over γ is demonstrated in the inset. We observed a linear dependence for larger values of γ , which however, deviates at the smaller γ .

4.2 Case with $b < 0$

Let us next focus on the ordering dynamics for quenches through the first-order line ($b < 0$) in Fig. 1. For $b < 0$, the first-order chiral phase transition occurs at $a < a_c = 3|b|^2/(16d)$. We consider quenches from the disordered state at $a > a_c$ ($M = 0$) to $a < a_c$. If we quench to $a < 0$, the free energy has a double-well structure, as shown in Fig. 1. Again, the ordering dynamics

is analogous to the previous case with $b > 0$. We have confirmed that the domain growth scenario is similar to that shown in Figs. 2–3. Subsequently, we focus only on quenches to $0 < a < a_c$. The appropriate form of the dimensionless time-dependent evolution equation reads

$$\frac{\partial^2}{\partial t^2} M + \gamma \frac{\partial}{\partial t} M = -M + M^3 - \lambda M^5 + \nabla^2 M + \theta(\vec{r}, t). \quad (9)$$

The free-energy extrema of the corresponding potential:

$$f(M) = \frac{1}{2}M^2 - \frac{1}{4}M^4 + \frac{\lambda}{6}M^6, \quad (10)$$

are located at $M = 0, \pm M_+$, and $\pm M_-$, where $M_+ = [(1 + \sqrt{1 - 4\lambda})/2\lambda]^{1/2}$ and $M_- = [(1 - \sqrt{1 - 4\lambda})/2\lambda]^{1/2}$. The extrema $M = 0, \pm M_+$ are the local minima with $f(\pm M_+) < f(0) = 0$ for $\lambda < \lambda_c$.

4.2.1 Short time behavior of the solution

First, we study the short time behavior of the solution of Eq. (9). We linearized it around the inflection point M_0 by replacing $M = M_0 + \phi'$ and average over the noise. To simplify the notation we use average fluctuation $\langle \phi' \rangle = \phi$. In Fourier space, the linearized equation becomes

$$\frac{\partial^2}{\partial t^2} \phi(\vec{k}, t) + \gamma \frac{\partial}{\partial t} \phi(\vec{k}, t) + [k^2 - |\alpha|] \phi(\vec{k}, t) = 0, \quad (11)$$

where $\alpha = (-1 + 3M_0^2 - 5\lambda M_0^4) < 0$ in our case. Equation (11) is a homogeneous second order differential equation and therefore one can write the general solution as

$$\phi(\vec{k}, t) = A_1 e^{A_1(\vec{k})t} + A_2 e^{A_2(\vec{k})t}. \quad (12)$$

Here A_1 and A_2 are integral constants and $\Lambda_1(\vec{k})$ and $\Lambda_2(\vec{k})$ are the roots of the quadratic equation: $\Lambda^2(\vec{k}) + \gamma\Lambda(\vec{k}) + (k^2 - |\alpha|) = 0$. The wavelengths for which $k^2 < \gamma^2/4 + |\alpha|$, roots are real, that give an exponential growth in the system instability. Similarly, for small wavelengths, in which $k^2 \gg \gamma^2/4 + |\alpha|$, we have imaginary roots that lead to oscillatory solutions, thus preventing the evolution of the system.

Further, in the strong dissipation limit ($\gamma \rightarrow \infty$), the short time solution of Eq. (11) is

$$\phi(\vec{k}, t) = A_0 e^{-(k^2 - |\alpha|)t/\gamma}. \quad (13)$$

Here one can see that for short wavelengths, where $k^2 > |\alpha|$, the fluctuations ϕ' decay with time, while those with $k^2 < |\alpha|$ grow exponentially. In this case the linear Eq. (11) is no longer valid and fully nonlinear Eq. (9) must be solved. However, without dissipation ($\gamma = 0$), the solutions of Eq. (11) become oscillatory, which prevent nucleation and growth in the system.

4.2.2 Phase plane analysis and bubble growth

Before we study the ordering dynamics of Eq. (9), it is instructive to understand the nature of the traveling-wave solutions. Our analytical understanding of the domain growth problem is based on the dynamics of domain interfaces (kinks and antikinks) that separate regions enriched in the two states $+M_+$ and $-M_+$. For the case with $b > 0$ and $a < 0$, discussed in Sec. 4.1, the kinks have tanh-profiles with small corrections in the potential due to the M^6 -term.

We consider the deterministic version of Eq. (9) in $d = 1$ as

$$\frac{\partial^2}{\partial t^2} M(z, t) + \gamma \frac{\partial}{\partial t} M(z, t) = -M + M^3 - \lambda M^5 + \frac{\partial^2}{\partial z^2} M. \quad (14)$$

We focus on traveling-wave solutions of this equation, $M(z, t) \equiv M(z - vt) \equiv M(\eta)$ with velocity $v > 0$. This reduces Eq. (14) to an ordinary differential equation:

$$(1 - v^2) \frac{d^2 M}{d\eta^2} + \gamma v \frac{dM}{d\eta} - M + M^3 - \lambda M^5 = 0. \quad (15)$$

Eq. (15) is equivalent to a 2- d dynamical system:

$$\begin{aligned} \frac{dM}{d\eta} &= y, \\ (1 - v^2) \frac{dy}{d\eta} &= M - M^3 + \lambda M^5 - \gamma v y. \end{aligned} \quad (16)$$

The phase portrait of this system will enable us to identify kink solutions of Eq. (14) with these relevant fixed points (FPs) $(M, y) = (0, 0)$, $(\pm M_-, 0)$, $(\pm M_+, 0)$ [13]. In Fig. 4, we show the phase portraits for $\lambda = 0.14$ ($< \lambda_c \simeq 0.1875$) and $v = v_s$, where v_s corresponds to the appearance of the saddle connections from $-M_+ \rightarrow 0$ and $+M_+ \rightarrow 0$. These correspond to kinks traveling with velocity $v_s > 0$, as shown in Fig. 4. Here, our analysis has been for the case with $v > 0$, but it is straightforward to extend it to the case with $v < 0$. In the latter case, the portrait in Fig. 4 is inverted, and the saddle connections (kinks) are from $0 \rightarrow -M_+$ and $0 \rightarrow +M_+$.

Next, we study the growth dynamics of a droplet. As we know that a first-order phase transition in QCD matter proceeds through a nonequilibrium process when the initial metastable phase breaks into droplets. In Fig. 5(a),

we show the growth of a droplet of the preferred massive phase ($M = +M_+$) in the background of the metastable phase ($M = 0$). It is obtained by solving Eq. (9) for $\lambda = 0.14$ and $\theta = 0$. In Fig. 5(b), we plot v_B vs. λ , where v_B is the bubble velocity. Our numerical data is in good agreement with v_s , which is obtained from the phase-plane analysis. We have done a detail analysis of bubble growth in Ref. [13].

In Fig. 6, the temporal variation of the order parameter field $M(\eta)$ is shown by solving Eq. (16) for $v_s = 0.66$ at four different values of γ . In the absence of dissipation ($\gamma = 0$), the solution of Eq. (16) is oscillatory (solid line) and therefore, it is difficult for the system to escape from the metastable state and nucleate and grow. However, as we increase the dissipation coefficient γ , it delays the time evolution of $M(\eta)$ to its vacuum value compared to the case with $\gamma = 0$. Therefore, a large dissipation (e.g., $\gamma = 1$) also prevents nucleation and growth in the system.

4.2.3 Chiral transition kinetics

Next, we consider the ordering dynamics of Eq. (9) from an initial disordered state. We follow the same numerical scheme used in Sec. 4.1. The initial state with massless quarks ($M = 0$) is now a metastable state of the potential. Therefore, the thermal noise $\theta(\vec{r}, t)$, which makes the system to escape from the metastable state have higher strength: $\epsilon = 2.4$. However, the asymptotic behavior of the domain growth in both the unstable and metastable cases is insensitive to the noise term [29, 30]. The chiral transition proceeds via the nucleation and growth of droplets of the preferred phase ($M = \pm M_+$).

In Fig. 7, we show the domain growth of the system for $\gamma = 0.25, 0.4$ and 0.5 . The frames are the cross-section of the 3- d snapshots at $z = N/2$ which show the evolution of one of the preferred phases ($M = M_+$) at times $t = 20, 50$ and 100 . Typically, the evolution of the system begins with the nucleation of droplets in the early stages. The droplets grow very rapidly and fuse to form bicontinuous domain structures, a characteristic of the late-stage domain growth. The effect of γ on the nucleation and growth can be easily understood by comparing the growth patterns at different γ values in Fig. 7. We observed that in shallow quenching through the first order line (I), the system takes more time to nucleate for the limiting γ values (i.e., $\gamma \rightarrow 0$ and $\gamma \rightarrow \infty$). However, for some moderate values ($\gamma = 0.4$), it takes less time.

In Fig. 8(a), we plot the scaled correlation function $[C(r, t) \text{ vs. } r/L]$ for the evolution shown in Fig. 7 at three different times. For figure clarity, we considered only two γ values 0.25 (open symbols) and 0.5 (filled symbols) respectively. At the early stages, the deviation of data sets, for both γ values, from the master curve reflect the morphological differences between the “nucleation and growth” and “domain coarsening”. As expected, scaling functions violate dynamical scaling in the crossover regime. However, at late time ($t = 100$) data sets collapse nicely onto a master curve for both γ values. The OJK function: $C(r, t) = 2/\pi \sin^{-1} \exp(-r^2/L^2)$ [31] has an excellent agreement with the master function. Therefore, the late-stage morphology in Fig. 7 is analogous to that for the unstable evolution, depicted in Fig. 2 (for $b > 0$). In Fig. 8(b), we plot the scaled structure factor $[L^{-3}S(k, t) \text{ vs. } kL]$ at the same times and for the same γ values as in Fig. 8(a). At late

times, the tail of the structure factor shows the Porod law, $S(k, t) \sim k^{-4}$ for $k \rightarrow \infty$ [32].

In Fig. 9, we show the domain size $[L(t) \text{ vs. } t]$ on a log-log scale. For a comparison, we plot for different values of γ . First, we observe that the growth process begins once the nucleation of the droplets are over. The asymptotic regime is once again described by the AC growth law, $L(t) \sim t^{1/2}$. Second, we find that the nucleation process is deeply affected by the dissipation coefficient γ . If we start from a moderate value of γ the time-span for the nucleation increases as $\gamma \rightarrow 0$ or $\gamma \rightarrow \infty$. Our simulation results also verify the analytical results obtained by Peter Hanggi in Ref. [33], where he described the dissipative escape of a particle from a metastable state, known as *Kramer's escape problem*.

5 Summary and Discussion

To conclude this paper, we summarize and discuss the results presented here. We have studied the kinetics of chiral phase transitions in *quantum chromodynamics* (QCD). At the microscopic level, these transitions are described by the NJL model. First, we have shown a quantitative mapping between the phase diagrams of the NJL model, which is an effective model of QCD at low energy, and the M^6 -Ginzburg Landau (GL) potential. This mapping enables us to identify the relevant time-scales and length-scales in QCD kinetics. Near the critical point, we associated (μ, T) and the coefficients of the GL model. However, we have considered parameter values far from the critical points, and it is more appropriate to interpret the GL coefficients as

phenomenological quantities.

We have studied the transitions from the massless quark (disordered) phase to the massive quark (ordered) phase, for different γ values resulting from a sudden quench in the temperature. We have considered both cases of the quench – deep quench as well as shallow quench. For deep quenches, the massless phase is spontaneously unstable and evolves into the massive phase via spinodal decomposition. In purely inertial case ($\gamma = 0$), we observed a rapid spinodal decomposition. Domains of massive phases do not relax to any equilibrium value due to oscillatory behavior of the system. However, they do with large γ values. The evolution morphologies show self-similar scaling, and can be quantitatively characterized by the order-parameter correlation function or its Fourier transform, the structure factor. The domain growth law is $L(t) \sim t^{1/2}$.

For shallow quenches, the massless phase is metastable. The system evolves via nucleation and the growth of droplets of the preferred phase. The dissipation factor γ affects the time-span for nucleation and growth. We observed that the nucleation time does not have any significant effect in the late-stage of the dynamics. Once the nucleation and growth of droplets is over, droplets quickly merge to form bicontinuous spatial domains which is analogous to the late-stage domain growth; the domain growth law is the AC law $L(t) \sim t^{1/2}$.

It is shown that a first-order phase transition in rapidly expanding matter should proceed through a far-from-equilibrium process when the initial metastable phase nucleated into droplets of massive phases. It would be quite

exciting to see if QCD matters undergo such a phase transition in relativistic heavy-ion collision experiments by making droplets of quark-gluon plasma.

Acknowledgment

AS thanks CSIR (India) for providing the financial support. The numerical work has been performed on the SPS cluster, JNU.

References

- [1] H. Caines, arXiv:nucl-ex/0906.0305 (2009).
- [2] B. Friman, C.H. Hne, J. Knoll, S. Leupold, J. Randrup, R. Rapp, P. Senger (eds.), Lect. Notes Phys. **814** (2011).
- [3] A.N. Sissakian and A.S. Sorin, J. Phys. G **36**, 064069 (2009).
- [4] A.J. Bray, Adv. Phys. **43**, 357 (1994).
- [5] B. Berdnikov and K. Rajagopal, Phys. Rev. D **61**, 105017 (2000).
- [6] D.T. Son and M.A. Stephanov, Phys. Rev. D **70**, 056001 (2004); H. Fujii, Phys. Rev. D **67**, 094018 (2003).
- [7] T. Koide, J. Phys. G **31**, 1055 (2005).
- [8] T. Koide and M. Maruyama, Nucl. Phys. A **742**, 95 (2004).
- [9] E.S. Fraga and G. Krein, Phys. Lett. B **614**, 181 (2005).
- [10] A. Bessa, E.S. Fraga and B.W. Mintz, Phys. Rev. D **79**, 034012 (2009).
- [11] V.V. Skokov and D. N. Voskresensky; Nucl. Phys. A **828** 401 (2009).
- [12] J. Randrup, Phys. Rev. C **79**, 054911 (2009); Phys. Rev. C **82**, 034902 (2010).
- [13] A. Singh, S. Puri, and H. Mishra, Nucl. Phys. A **864**, 176 (2011).
- [14] P.C. Hohenberg and B.I. Halperin, Rev. Mod. Phys **49**, 435 (1977).

- [15] D. Boyanovsky, H.J. de Vega, R. Holman, and J. Salgado, Phys. Rev. D **59**, 125009 (1999).
- [16] M. Gleiser and R.O. Ramos, Phys. Rev. D **50**, 2441 (1994).
- [17] D.H. Rischke, Phys. Rev. C **58**, 2331 (1998).
- [18] W. Fu, D. Huang and F. Wang, Nucl. Phys. A **849**, 203 (2011).
- [19] M. Nahagang, S. Leupold, C. Herold and M. Bleicher, Phys. Rev. C **84**, 024912 (2011).
- [20] M. Nahagang, S. Leupold, and M. Bleicher, arXiv:nucl-th/1105.1396 (2011).
- [21] M. Nahagang, M. Bleicher, S. Leupold, I. Mishustin, arXiv:nucl-th/1105.1962 (2011).
- [22] M. Asakawa, and K. Yazaki, Nucl. Phys. A **504**, 668 (1989).
- [23] C. Sasaki, B. Friman, and K. Redlich, Phys. Rev. D **77**, 034024 (2008).
- [24] M. Iwasaki, Phys. Rev. D **70**, 114031 (2004).
- [25] S. Puri, and V.K. Wadhawan (eds.), *Kinetics of Phase Transitions*, CRC Press, Boca Raton, Florida (2009).
- [26] D.H. Rischke, Phys. Rev. C **58**, 2331 (1998).
M. Gleiser and R.O. Ramos, Phys. Rev. D **50**, 2441 (1994).
- [27] H. Heiselberg, C.J. Pethick and E.F. Staubo, Phys. Rev. Lett. **70**, 1355 (1993).

- [28] K. Kajantie, Phys Lett. B **285**, 331 (1992).
- [29] Y. Oono and S. Puri, Phys. Rev. Lett. **58**, 836 (1987); Phys. Rev. A **38**, 434 (1988); S. Puri and Y. Oono, Phys. Rev. A **38**, 1542 (1988).
- [30] S. Puri and Y. Oono, J. Phys. A **21**, L755 (1988).
- [31] T. Ohta, D. Jasnow, and K. Kawasaki, Phys. Rev. Lett. **49**, 1223 (1982).
- [32] G. Porod, in *Small-Angle X-Ray Scattering*, O. Glatter, and O. Kratky, Eds., Academic Press, NewYork, **42** (1982).
- [33] P. Hanggi, J. Stat. Phys **42**, 105 (1986).

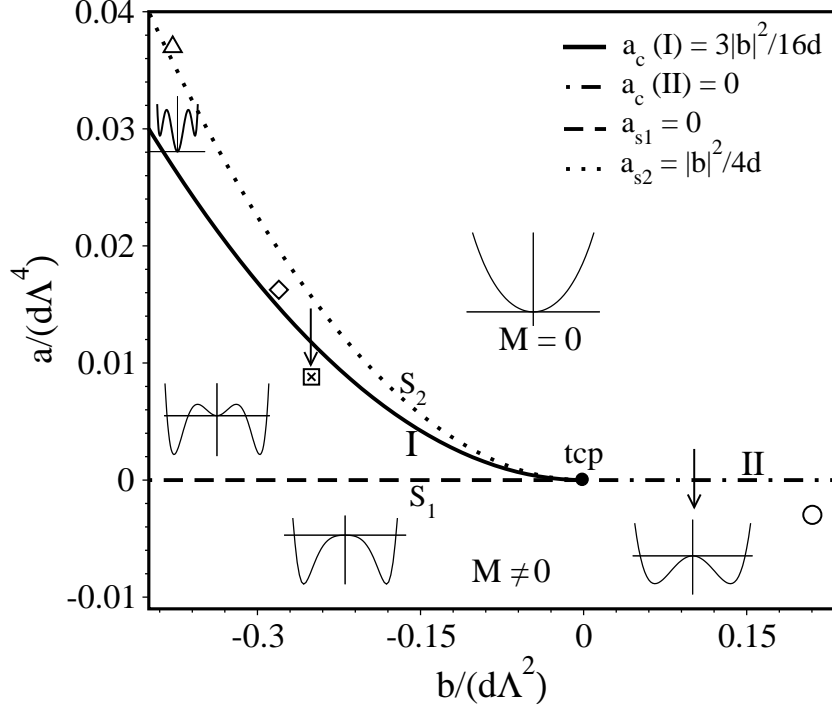


Figure 1: Phase diagram for the Landau free energy in Eq. (2) in the $[b/(d\Lambda^2), a/(d\Lambda^4)]$ -plane, where we have set the three-momentum ultraviolet cutoff $\Lambda = 653.3$ MeV. A line of first-order transitions (I) meets a line of second-order transitions (II) at the tricritical point (tcp), which is located at the origin. The equation for I is $a_c = 3|b|^2/(16d)$, and that for II is $a_c = 0$. The dashed lines denote the spinodals S_1 and S_2 , with equations $a_{S_1} = 0$ and $a_{S_2} = |b|^2/(4d)$. The typical forms of the Landau potential in various regions are shown in the figure. The cross denotes the point where we quench the system for $b < 0$. The point $b/(d\Lambda^2) = 1.269$, $a/(d\Lambda^4) = -0.225$ corresponds to the second order quench. We do not mark this point in the figure as it results in a loss of clarity. The open symbols denote 4 combinations of $(b/(d\Lambda^2), a/(d\Lambda^4))$, chosen to represent qualitatively different shapes of the GL potential.

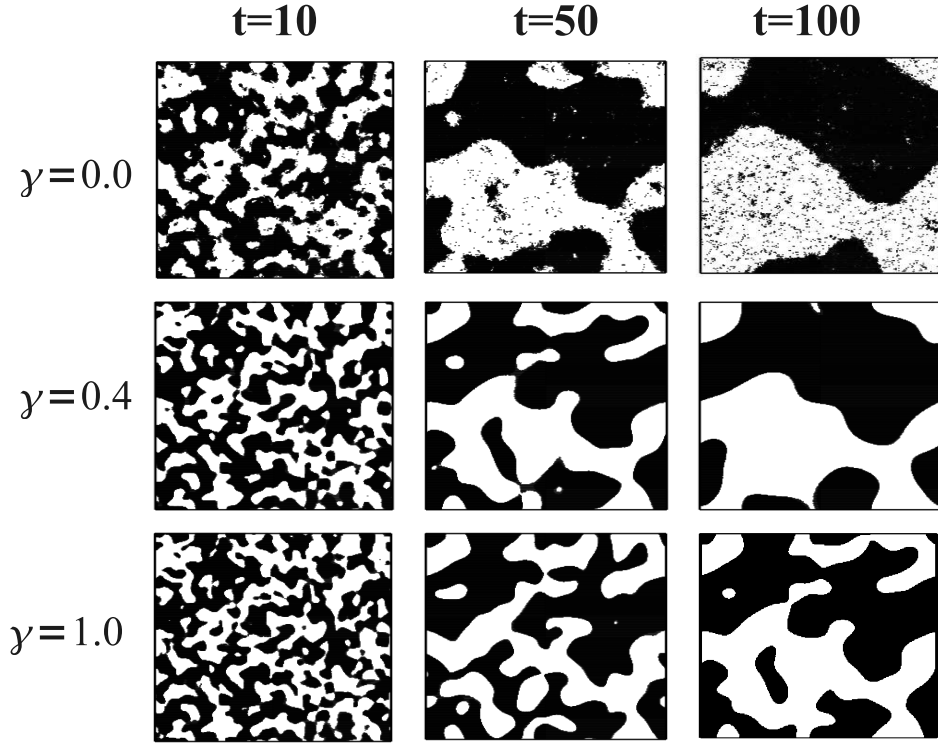


Figure 2: Domain evolution of a preferred massive phase ($M = M_+$) after a deep temperature quench [through the second-order line (II) in Figs. 1] for three different values of γ . The frames are the cross-section of the 3- d snapshots at $z = N/2$ for $t = 10, 50$ and 100 obtained by numerically solving Eq. (8) with $a < 0$, $b > 0$, $\lambda = 0.14$. The noise strength is $\epsilon = 0.008$.

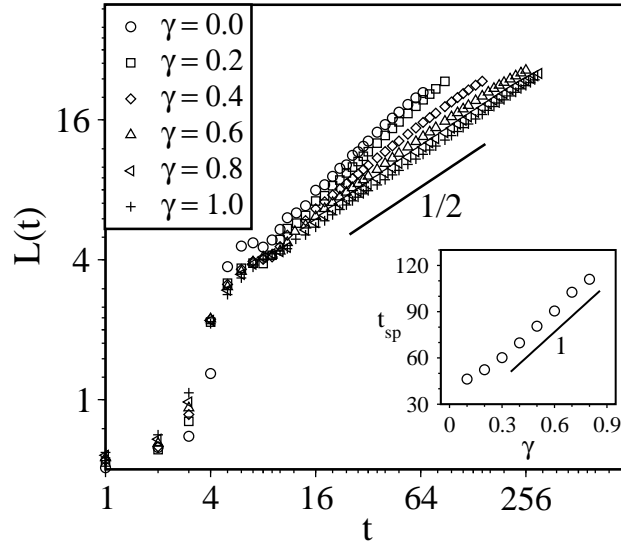


Figure 3: Time-dependence of domain size, $L(t)$ vs. t , for the evolution in Fig. 2. The length scale $L(t)$ is defined as the distance over which $C(r, t)$ decays to half its maximum value. The coarsening process obeys the Allen-Cahn (AC) growth law, $L(t) \sim t^{1/2}$ for larger values of γ , such as 0.6, 0.8 and 1.0 respectively. However, for smaller $\gamma = 0, 0.2$ we observed an explosive domain growth with higher growth exponent.

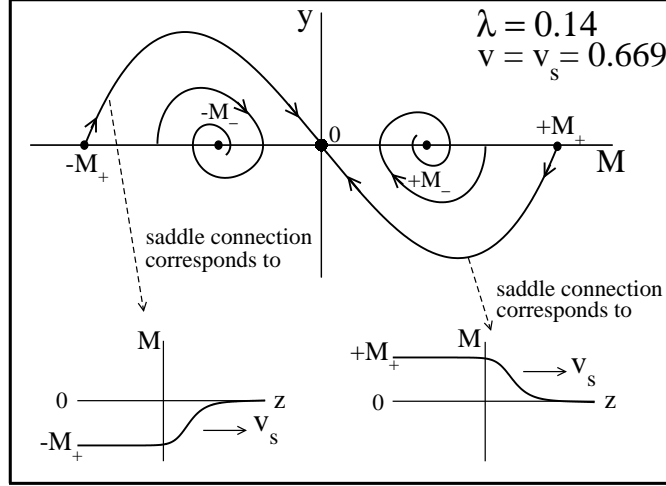


Figure 4: Phase portraits of the dynamical system in Eq. (16) for $\lambda = 0.14$. The phase portrait for $v_s = 0.6690$, where v_s corresponds to the appearance of the saddle connections from $-M_+ \rightarrow 0$ and $+M_+ \rightarrow 0$. These correspond to kinks traveling with velocity $v_s > 0$.

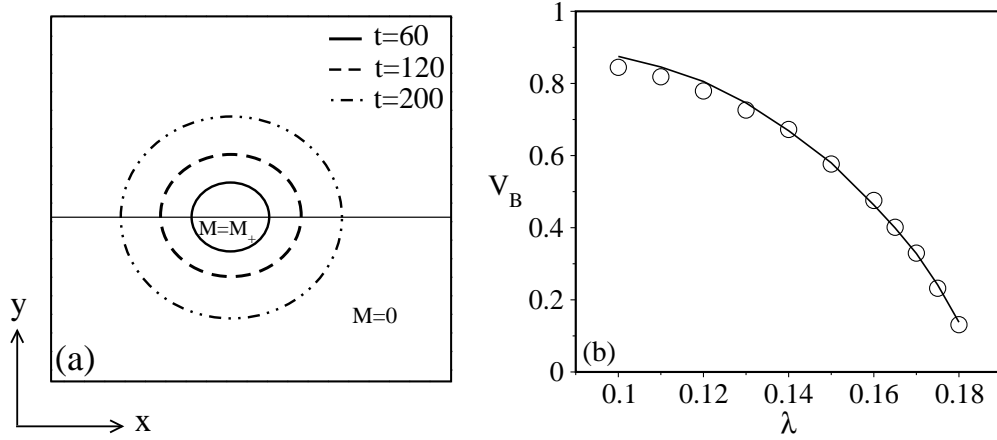


Figure 5: (a) Growth of droplet of the preferred phase ($M = +M_+$) in a background of the metastable phase ($M = 0$) for $\lambda = 0.14$. We show the boundary of the droplet at three different times. The innermost circle corresponds to a droplet at time, $t = 20$ (b) Plot of the bubble growth velocity v_B vs. λ . The circles refer to the numerical data, while the solid line corresponds to the result from a phase-plane analysis.

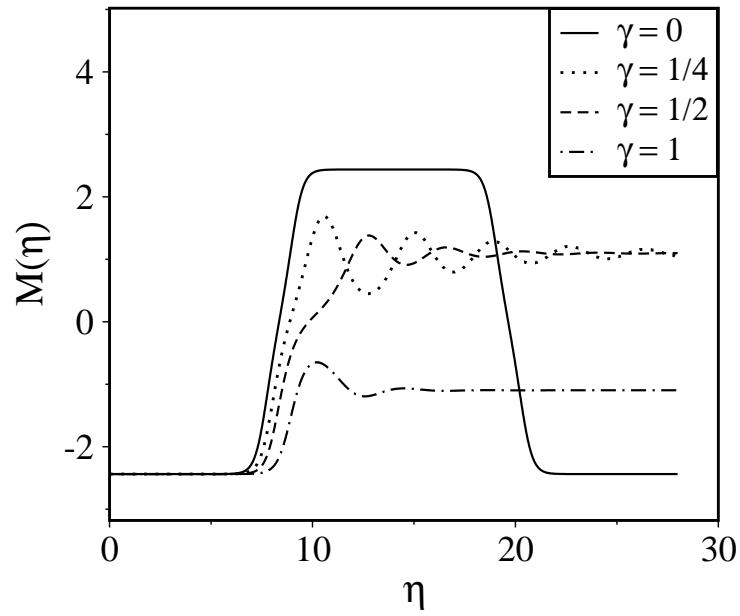


Figure 6: Temporal variation of the order parameter field $M(\eta)$ as a function of η for four different values of γ . Without dissipation ($\gamma = 0$), the solution of Eq. (16) is oscillatory [solid line] and therefore it is difficult for the system to nucleate and grow.

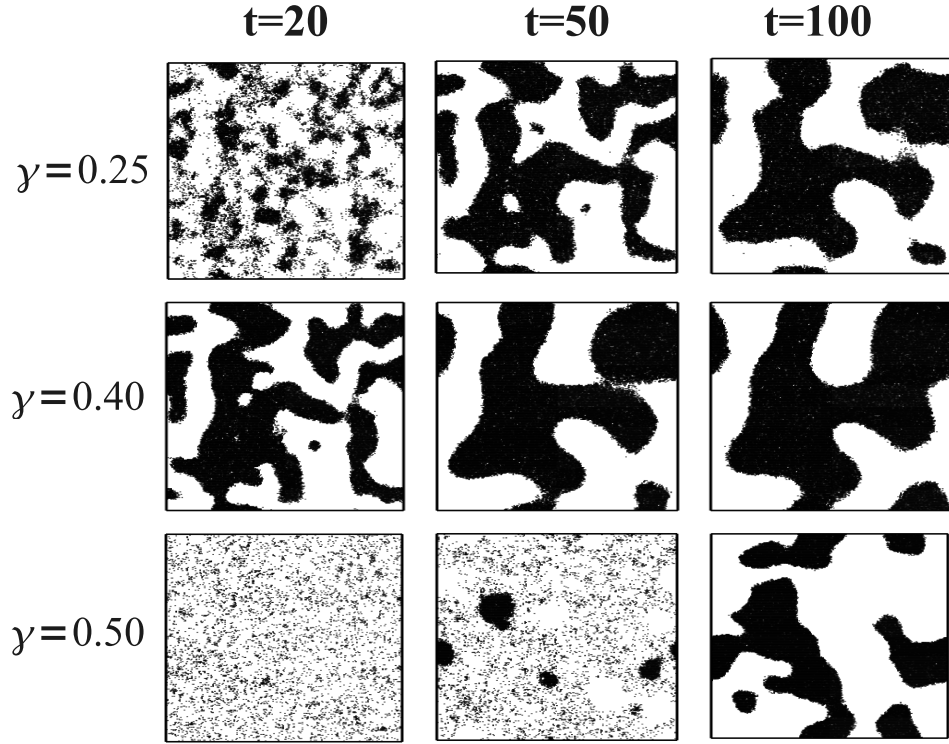


Figure 7: Domain evolution after a shallow temperature quench [temperature quench through the first-order line (I) in Figs. 1] for $\gamma = 0.25, 0.4$ and 0.5 respectively. The cross-section of the 3- d snapshots at $z = N/2$ show the evolution of preferred phases with $M = +M_+$ at times $t = 20, 50$ and 100 , respectively. For a moderate γ , nucleation is faster (e.g., at $\gamma = 0.4$) than the other two limiting γ values.

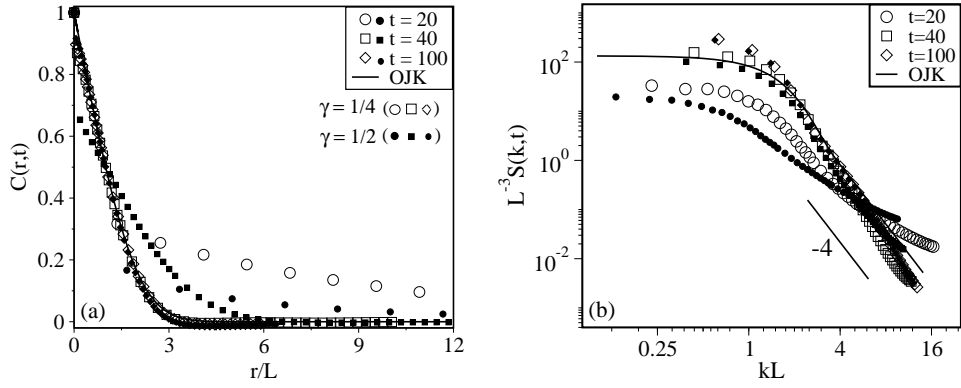


Figure 8: (a) Scaling of the correlation function $[C(r,t)$ vs. $r/L]$ for the evolution shown in Fig. 7 at three different times. At early stages, the deviation of data sets from the master curve reflect the morphological differences between the “nucleation and growth” and “domain coarsening”. However, at late time ($t = 100$) data sets collapse nicely onto a master curve for both γ values. The OJK function has an excellent agreement with the simulation result. (b) Scaling plot of the structure factor $[L^{-3}S(k,t)$ vs. $kL]$ for the same times as in (a). At late times, the tail of the structure factor shows the Porod law, $S(k,t) \sim k^{-4}$ for $k \rightarrow \infty$.

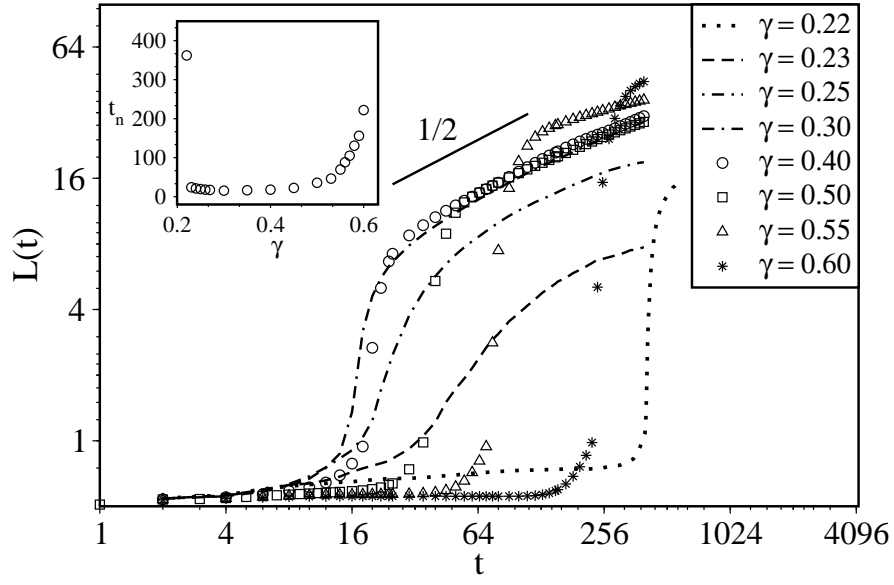


Figure 9: (a) Time-dependence of the domain size $L(t)$ vs t for different γ values. There is no growth in the early stages when droplets are being nucleated. It also reflects the effect of dissipation on the nucleation and growth process. However, The asymptotic regime of the domain growth is consistent with the AC growth law, $L(t) \sim t^{1/2}$.